Received: 11 March 2025 | Revised: 7 May 2025 | Accepted: 15 May 2025

DOI: 10.1002/alz.70368

Alzheimer's & Dementia®
THE JOURNAL OF THE ALZHEIMER'S ASSOCIATION

RESEARCH ARTICLE

Increased activity of Piezo1 channel in red blood cells is associated with Alzheimer's disease-related dementia

Valeriia Sitnikova[1] | Dilyara Nurkhametova[1] | Nicoletta Braidotti[2,3] | Catalin D. Ciubotaru[2] | Luca Giudice[1] | Ulla Impola[4] | Sari Kärkkäinen[5] | Juho Kalapudas[6] | Elina Penttilä[7] | Heikki Löppönen[7] | Ilkka Fagerlund[1] | Katja M. Kanninen[1] | Henrik Zetterberg[8,9] | Tarja Kokkola[10] | Saara Laitinen[4] | Anne Koivisto[6,10] | Dan Cojoc[2] | Rashid Giniatullin[1] | Tarja M. Malm[1]

[1]A.I. Virtanen Institute for Molecular Sciences, University of Eastern Finland, Kuopio, Finland

[2]Materials Foundry, National Research Council of Italy (CNR-IOM), Area Science Park Basovizza, Trieste, Italy

[3]Department of Physics, University of Trieste, Trieste, Italy

[4]Research and Development, Finnish Red Cross Blood Service, Helsinki, Finland

[5]Biomarker Laboratory, Institute of Clinical Medicine/Neurology, University of Eastern Finland, Kuopio, Finland

[6]Neuro Centre, Kuopio University Hospital, Kuopio, Finland

[7]Department of Otorhinolaryngology, School of Medicine, University of Eastern Finland, and Kuopio University Hospital, Kuopio, Finland

[8]Clinical Neurochemistry Laboratory, Sahlgrenska University Hospital, Göteborg, Sweden

[9]Department of Psychiatry and Neurochemistry, Institute of Neuroscience and Physiology, the Sahlgrenska Academy at the University of Gothenburg, Göteborg, Sweden

[10]Department of Geriatrics and Neurological Memory polyclinic, Helsinki University Hospital and Neurosciences, Faculty of Medicine, University of Helsinki, Helsinki, Finland

Correspondence
Valeriia Sitnikova and Tarja M. Malm, A.I. Virtanen Institute for Molecular Sciences, University of Eastern Finland, Neulaniementie 2, Bioteknia 1, Office 3206, Kuopio, Finland.
Email: valeriia.sitnikova@uef.fi and tarja.malm@uef.fi

Present address
Nicoletta Braidotti, Department of Chemical and Pharmaceutical Sciences, University of Trieste, Trieste, Italy

Funding information
Swedish State Support for Clinical Research, Grant/Award Number: ALFGBG-71320; HORIZON EUROPE European Research Council, Grant/Award Number: 101053962;

Abstract

INTRODUCTION: Red blood cells (RBCs) are crucial for oxygen delivery to active tissues and endure significant mechanical forces in the microcirculatory bed. The enrichment of mechanosensitive Piezo1 channels, linked to the cytoskeleton, aids RBCs in navigating the narrow capillaries. In Alzheimer's disease (AD), impaired brain microcirculation may necessitate enhanced Piezo1 function in RBCs.

METHODS: With micropipette aspiration and flow cytometry technics, we evaluated, using the specific Piezo1 agonist Yoda1, AD-related alterations in the biomechanical properties of RBCs from cognitively healthy patients (HC) and individuals with mild cognitive impairment (MCI) and AD.

RESULTS: We show that beta-amyloid (Aβ) peptides alter the biomechanical properties of RBCs. We observed significantly higher Yoda1-induced calcium responses in RBCs in individuals with MCI and AD compared to RBCs from age-matched HC.

Swedish Research Council, Grant/Award Numbers: 2023-00356, 2022-01018, 2019-02397; Business Finland; Academy of Finland

CONCLUSION: Our data suggest that Yoda1-induced Ca^{2+} flux through Piezo1 channel emerges as a measurable indicator associated with and improves the detection of AD-related dementia.

KEYWORDS
Alzheimer's disease, Ca-imaging, Piezo1, RBC

Highlights

- Piezo1 channels aid the navigation of red blood cells (RBCs) through narrow capillaries.
- Alzheimer's disease (AD) patients show increased Yoda1-induced activation of Piezo1 in RBCs.
- Incorporation of Yoda1-induced Piezo1 readouts improved the detection of AD-related dementia.
- Investigating Yoda1-induced Piezo1 activity associated with early AD.

1 | BACKGROUND

Red blood cells (RBCs) or erythrocytes are specialized cells that undergo substantial changes during maturation, shedding off most of their organelles and intracellular machinery. During maturation, RBCs lose their nuclei and acquire a biconcave shape.[1] They play a pivotal role in gas exchange by transporting oxygen to all cells and tissues and by carrying carbon dioxide back to the lungs. Over their approximately 120-day lifespan, human RBCs constantly circulate through the bloodstream and interact with a diverse array of cell types. Owing to their remarkable flexibility, RBCs can adapt their shape to traverse the narrowest capillaries throughout the bloodstream. This is facilitated by highly mechanosensitive, calcium-permeable Piezo1 channels that control RBCs' volume homeostasis in close cooperation with Gárdos K^+ channels.[2–4] Studies suggest that Piezo1 channel distribution on RBC membrane is non-uniform, with a preference for regions with higher curvature.[5] Although RBCs have relatively low number of Piezo1 channels per RBC,[5] their strategic localization and high reactivity to mechanical stress ensure proper RBC function.

Recent data obtained by us[6] and others[7] suggested that changes in Piezo1 function are associated with Alzheimer's disease (AD). Piezo1 is prominently expressed in multiple cell types, and it regulates many vital functions of microglia[6] and astrocytes[8]. Notably, the expression of Piezo1 in microglia[6] and in astrocytes[8] is altered in AD brain. These data suggest that the function of Piezo1 can reflect the progression of this disorder. While the mechanisms of how Piezo1 is involved in AD pathogenesis are unknown, we, together with others, have demonstrated that beta-amyloid protein (Aβ) in small concentration inhibits the proper function Piezo1 channel.[6,9,10]

Since their discovery, misfolded and aggregated Aβ peptides have been associated with AD pathology. It has been shown that levels of the 42-residue form of beta-amyloid peptide (Aβ42) in cerebrospinal fluid (CSF) and plasma decrease upon the pathological progression of AD, except for individuals with familial AD, whose plasma levels of Aβ are elevated upon the progression of dementia.[11–13] While the reduced levels of CSF Aβ have been shown to more accurately associate with the cognitive decline in AD,[11,12] the levels in plasma have yielded more controversial results, given significant variations and very low concentrations of Aβ in plasma.[12,14–16]

Alterations in RBCs can serve as diagnostic indicators in various medical conditions, reflecting significant ongoing physiological perturbations within the human body. It has been shown that Piezo1 channels play an important role in the regulation of RBC volume[2,17] and their activation in RBCs has been linked to changes in the cell shape and deformability.[2,18,19] This is crucial for the ability of RBCs to squeeze through narrow blood vessels and effectively deliver oxygen. Notably, brain microcirculation is essentially impaired in AD.[20,21] RBC deformability can also be disabled due to mutation of *piezo1* in erythrocyte-form-changing diseases such as hereditary xerocytosis.[2,22]

Prior studies have shown that interaction of RBCs and Aβ can affect RBC membrane fluidity and integrity, potentially leading to changes in the shape and function of RBCs.[23–25] Some studies have suggested that Aβ can promote aggregation of RBCs, leading to the formation of clumps. This aggregation can affect blood flow and potentially contribute to microcirculatory issues in AD.[23,26,27] There is also evidence that amyloid has a lytic effect on RBCs and can bind to hemoglobin within RBCs.[25] This interaction may have implications for oxygen transport and could contribute to altered RBC function. In AD, Aβ can accumulate in blood vessels, leading to a condition known as cerebral amyloid angiopathy (CAA).[28] CAA can affect blood vessel integrity and may indirectly impact RBCs' ability to deliver oxygen to the brain.

Considering the important role of Piezo1 channels in RBC homeostasis and the proposed association between Aβ and Piezo1 in the context of AD, we evaluated whether the Piezo1 channel activity is altered in patients with early AD-related dementia.

2 | METHODS

Blood samples for the study have been donated from the Kuopio University Hospital (KUH) (APOLLO cohort), Red Cross (Helsinki), and Azienda Sanitaria Universitaria Giuliana Isontina (ASUGI, Trieste).

2.1 | Study cohort

The discovery cohort (named APOLLO) included plasma samples of AD (N = 32), and non-demented patients (N = 70) recruited via KUH. AD diagnosis of the study patients had been made before the study recruitment at the KUH using 2017 National Care guideline recommendations for diagnosing AD. These criteria were based on 2011 revised National Institute of Neurological and Communicative Disorders and Stroke and the Alzheimer's Disease and Related Disorders Association (NINCDS-ADRDA) criteria.[29] All AD cases had AD phenotype and evidence of neurodegenerative changes in magnetic resonance imaging (MRI) or in fluorodeoxyglucose-positron emission tomography (FDG-PET) typical to AD. The AD patients had early (total Clinical Dementia Rating scale [CDR] score 0.5) or mild (total CDR score 1) stage AD.

All study patients, both non-demented and AD patients, underwent the Consortium to Establish a Registry for Alzheimer's Disease neuropsychological test battery (CERAD-NB) and interviews: demographic and CDR, interview, which included six different dimensions.[30,31] Both the study patient and family members were interviewed. CDR combined information about cognition and daily function. The APOLLO cohort grouping was based on these evaluations. The non-demented study patients (N = 70) were shared to the cognitively healthy controls (HC, N = 31) or to MCI group (N = 39). The MCI group study patients had objective cognitive impairment (amnestic or non-amnestic) on the basis of the CERAD-NB but had not deteriorated in their everyday daily functions reflecting the total CDR score 0.5. The HCs had performed cognitive tests within normal range and they performed their daily tasks normally (the total CDR score 0).

Blood samples were genotyped for apolipoprotein E (*APOE*) ε2, ε3, and ε4 alleles (Table 1). All the participants also passed through clinical blood tests, including complete blood count (CBC) parameters, lipid profile, and basic metabolic panel parameters (glucose, Na^+, K^+, Ca^{2+}) (Table S1). In the APOLLO cohort, participants were excluded if they had any uncompensated disease, confirmed by the clinical blood test results.

2.2 | Blood sample collection and processing

Blood samples were freshly collected from median cubital vein in Vacutainer tubes K2E (BD Vacutainer, UK) with ethylenediaminetetraacetic acid (EDTA) as anticoagulant.

Sample processing was performed immediately after blood was collected. In case of visible aggregates, the sample was filtered through 100 µM CellTrix filter. The blood samples (150 µL) were washed two times with phosphate buffered saline (PBS) (5 min, 300 g, room temperature [RT]) to remove plasma and anticoagulant. After centrifugation, 50 µL of red blood cells were transferred to clean tube and resuspended in 200 µL PBS (250 µL total volume of cell suspension). 2X Fluo-4 dye (Invitrogen, F10471) 250 µL (1:1) was added and cells were incubated for 30 min at 37°C in dark. After the incubation sample was washed twice with PBS and once with Hank's balanced salt solution (HBSS; 5 min, 300 g, RT). Supernatant was carefully removed with transfer pipette and 50 µL pellet was resuspended in 450 µL of HBSS to form 10% cell suspension. Ten microliter of 10% cell suspension was transferred to 390 µL of RPMI buffer (RPMI [Gibco, 11835030] +1% of FBS [Gibco, 10270106]) and used for flow-cytometry analysis.

RESEARCH IN CONTEXT

1. **Systematic review**: Red blood cells (RBCs) are essential for oxygen delivery and endure significant mechanical forces in the microcirculatory bed. The enrichment of mechanosensitive Piezo1 channels, linked to the cytoskeleton, aids RBCs in navigating narrow capillaries. Alzheimer's disease (AD), the most common cause of dementia in the elderly, is characterized by impaired brain microcirculation, which may necessitate enhanced Piezo1 function in RBCs.
2. **Interpretation**: We discovered increased Yoda1-induced calcium flux and changes in the biomechanical properties of the membrane in RBCs of AD patients. Incorporation of the Piezo1-driven Ca2+ responses into random forest classifier significantly improved the detection of AD-related dementia.
3. **Future directions**: Piezo1 receptors have not yet demonstrated their full potential as indicators of calcium signaling in AD. Assessing Piezo1 calcium currents as part of routine AD diagnostic tests may contribute to earlier disease detection.

2.3 | Flow cytometry time-lapse analysis of Piezo1-mediated Ca^{2+}-flux

We used flow cytometry to determine the time-course of the Yoda1-mediated response in Fluo4 1X loaded RBCs. Samples were analyzed using CytoFLEX S flow cytometer (Beckman Coulter). This flow cytometer is equipped with peristaltic pump, which allowed the application of the Piezo1 agonist Yoda1 during data acquisition. After 20-s recording (baseline fluorescence), the Yoda1 at 5 µM concentrations was applied, following by 4 min recording and addition of ionomycin (10 µM) at 4 min 20 s recording, as positive control. Fluo4 fluorescence was measured by using median fluorescence intensity (MFI) of single cells at different time points—baseline (before application of

TABLE 1 Numerical values of SIMOA and Ca^{2+} max amplitude measurements.

Characteristic	HC	MCI	AD	*p*-value
Aβ40 pg/mL (mean ± SD)	118.10 ± 15.66	118.00 ± 22.18	125.60 ± 35.58	0.6338
Aβ42 pg/mL (mean ± SD)	6.75 ± 1.37	6.35 ± 2.03	6.07 ± 1.88	0.0235
GFAP pg/mL (mean ± SD)	149.10 ± 66.10	146.70 ± 61.91	205.60 ± 100.50	0.0091
NfL pg/mL (mean ± SD)	24.85 ± 7.50	24.86 ± 28.41	30.38 ± 14.02	0.0304
pTau231 pg/mL (mean ± SD)	9.14 ± 3.84	10.54 ± 3.84	10.38 ± 3.48	0.0696
Max Ca^{2+} response from Piezo1 receptors (mean ± SD)	7.74 ± 2.10	9.38 ± 1.69	10.21 ± 2.44	<0.0001
Max Ca^{2+} response from Piezo1 receptors (median ± SD)	10.22 ± 2.51	11.88 ± 2.05	12.75 ± 2.70	0.0001

Abbreviations: Aβ40 and Aβ42, beta-amyloid peptides; AD, Alzheimer's disease; Ca, calcium; GFAP, glial fibrillary acidic protein; HC, healthy controls; MCI mild cognitive impairment; NfL, neurofilament light chain; SIMOA, single-molecule assay.

Yoda1) and every 20 s after Yoda1 application. Sample preparation and flow cytometry analysis were performed blinded. Between samples, the flow cytometer was washed to prevent fluorescent cells cumulation and bias. The gating strategy of the samples is demonstrated in Figure S1.

2.4 | Flow cytometry scattered signals analysis of Piezo1-mediated Ca-flux

Together with the time-lapse analysis of samples, optical parameters were analyzed, using CytoFLEX S flow cytometer (Beckman Coulter). We chose area measurement (SSC-A and FSC-A) as one having the best correlation to the cell size and the most complete and realistic cell scenario.[32] We measured median FSC-A and SSC-A for the RBCs at the BL and under Yoda1 treatment, when the Ca^{2+} reached maximum amplitude (Figure S2). After that, the differences between SSC-A for BL and Yoda1 and FSC-A for the same time points have been calculated and transferred to percentages. Then, these percentages have been compared between groups of patients.

2.5 | Imaging flow cytometry

On average, over 5000 red blood cells of each sample were characterized using Amnis ImageStreamX Mk II Imaging Flow Cytometer (Luminex, Cytek Biosciences). The gating strategy of the samples is demonstrated in Figure S3. Excitation lasers 488 and 785 nm and 60x magnification were used for data collection. Channels Ch01 and Ch09 were used for the bright field (BF), Ch06 for side scattering, and channel Ch02 for the fluorescence signal detection. All data were analyzed using *IDEAS* 6.2 Image Data Exploration and Analysis Software.

2.6 | Simoa Neuro4-Plex E assay

Plasma concentrations of Aβ40, Aβ42, glial fibrillary acidic protein (GFAP), and neurofilament light chain (NfL) were measured using the Single molecule array (Simoa) Neurology 4-Plex E Advantage kit (103670, Quanterix, Billerica, Massachusetts, USA) on an HD-X analyzer according to manufacturer's instructions.

2.7 | pTau231 measurement

Plasma pTau231 concentration was measured using an in-house Simoa assay as previously described.[33]

2.8 | Micropipette aspiration

RBC preparation was performed the same way as described above. After staining, we diluted cells to 1% suspension, and 10 µL cells were resuspended in 1 mL of (HBSS:RPMI buffer as 1:1). From 1% suspension, 5 µL of cells were taken to 400 µL of recording buffer (HBSS:RPMI buffer as 1:1). These additional dilutions have been made to get good imaging density of the cells. Cells in recording buffer were loaded with 1 µM Aβ (Bachem) or vehicle (dimethyl sulfoxide [DMSO]) and left into darkness for 20 min for incubation. After these steps, micropipette aspiration has been performed.

The micropipette aspiration and multimodal imaging system and the measurement of the elasticity and viscosity are described in Braidotti et al.[34] Briefly, the aspiration was performed by using a tapered borosilicate glass capillary (1–3 µm in diameter at the tip). A microfluidic pump (Flow ZE, Fluigent, France), which allows to create negative pressures for cells aspiration, was controlled by custom software. BF and fluorescence imaging are implemented in parallel on an optical inverted microscope (Olympus IX81) working with 60 × 1.4 NA oil objective (Olympus). The two imaging channels are recorded at seven frames per second on a CCD dual sensor camera (Orca-D2, Hamamatsu) for monitoring cells deformation and Ca^{2+} gating, respectively.

A glass capillary tube was filled with the recording buffer and placed near the cell. By decreasing stepwise, the negative pressure with step of 0.5 mbar/s a single cell is aspired at a time. Recording starts just before the application of negative attractive pressure and lasts till the RBC is completely sucked into the pipette.

Mechanical parameters such as Young's Modulus and cell viscosity have been retrieved from cell deformation (using BF imaging) against

pressure recorded during aspiration as described in Braidotti et al.[34] The activation pressure, as defined in Braidotti et al., [34] has been evaluated from the recorded florescence signal versus pressure.

2.9 | Random Forest classification

We conducted the classification of the dataset comprising 74 individuals divided into three classes of patients: AD, HC, and MCI. The dataset included 47 features among clinical variables (e.g., Age, Gender, BMI, HbA1c), MRI variables (e.g., hippocampus_right, temporal_lobe_right), CERAD variables (e.g., Word recall, Tot_Memory_Score), and Piezo1 channel Ca^{2+} measurements. We then extracted the importance of the features, the best feature interactions, and the proximity matrix from the trained models (Supplementary Data 1). Finally, we performed the re-classification of the dataset without Piezo1 channel Ca^{2+} measurements to compare the trained models (Supplementary Data 2).

The analysis was implemented using R and multiple packages, including caret,[35] randomForest,[36] randomForestExplainer, and PRROC. The random forest classifier was trained and evaluated using a nested cross-validation approach with five folds and two iterations, resulting in 10 independent training and testing sets. Hyperparameter tuning was performed within each training set to optimize mtry (number of variables randomly sampled as candidates at each split) and nodesize (minimum size of terminal nodes). The final model was trained using optimal hyperparameters and 3000 trees. Missing values were imputed using missForest (blind imputation)[37] for testing sets and either missForest (blind imputation) or mice (informed by the target variable)[38] for training sets, depending on the accuracy of the imputation. Random Forest classification output is presented in Supplementary data 1 and Supplementary data 2.

2.10 | Statistical analysis

Data were analyzed using CytExpert 2.3 software and GraphPad Prism 8 (GraphPad Software, La Jolla, California, USA). Statistical analyses have been chosen based on data distribution. In case of normal distribution, ANOVA statistical tests have been performed followed by Bonferroni's multiple comparisons test. In other case, nonparametric Mann-Witney U-test and Kruskall-Wallis tests have been accomplished. Differences with p values of less than 0.05 were considered statistically significant. The data are presented as mean ± SEM.

3 | RESULTS

3.1 | Aβ-induced changes in biomechanical properties of RBCs

We first explored the impact of Aβ on biomechanical properties of RBCs of healthy volunteers. To this end, we employed a recently validated approach based on the combination of multimodal imaging and micropipette aspiration.[34] We applied micropipette aspiration technique, mimicking the deformation of RBCs in capillary bed[34,39,40] to measure cell deformation and Ca^{2+} influx through mechanosensitive channels confirming prominent Yoda1 induced Ca^{2+} influx (Figure 1A, B). The level of calcium responses was evaluated in vehicle-treated RBCs and in RBCs exposed to 1 μM Aβ42. RBCs incubated with Aβ required higher activation pressure to trigger Ca^{2+} influx through Piezo1 channels compared to vehicle treated RBCs (Figure 1C, D). Application of 1 μM Aβ increased the activation pressure (Figure 1C, D), however, induced a significant decrease in Young's Modulus and membrane viscosity of the RBCs (Figure 1E, F), suggesting that Aβ alters the biomechanical properties of RBCs.

3.2 | Aβ decreased Yoda1-induced calcium responses in RBC

To evaluate further whether these responses were related to RBC morphology, we imaged the Yoda1-induced responses in the presence or absence of Aβ at micromolar, nanomolar, and picomolar concentrations in single RBCs using Amnis ImageStreamX MkII imaging flow cytometer (Amnis). The advantage of the imaging flow cytometer is the ability for real-time detection of both the morphology and fluorescent signal of every cell passing through the laser (Figure 2A). Pre-incubation of RBCs with Aβ led to dose-dependent decrease in the percentage of Yoda1 induced fluorescent cells (Figure 2B) and visible Yoda1-induced alterations in RBC morphology.

3.3 | RBCs from MCI and AD patients show enhanced Yoda1-induced Ca^{2+} flux

To address if the activation properties of Piezo1 are altered in RBC in AD, we measured Yoda1-induced calcium responses in RBC from age-matched HCs, individuals with MCI and patients diagnosed with AD. Calcium responses were recorded using CytoFlex flow cytometer (Beckman Coulter) in a time-lapse mode after application of Yoda1 at 5 μM concentration chosen based on our previous studies.[6] We detected a significant increase in the amplitude of Ca^{2+} response in both the patients with MCI and AD compared to HCs in tested concentration (Figure 3). However, the response failed to reach statistical significance between patients with MCI and AD suggesting an early increase in Yoda1 responsiveness during the disease.

3.4 | RBCs from MCI and AD patients show alterations in their morphological characteristics as analyzed by flow cytometry

Considering that the biomechanical properties of RBCs are altered in the presence of Aβ, and that Piezo1 receptor activity is increased in AD and MCI patients, we analyzed scatter properties of the Yoda1-treated RBCs in the flow-cytometry data. SSC generally reflects cell complexity (granularity), but in the case of RBCs, we associated it with

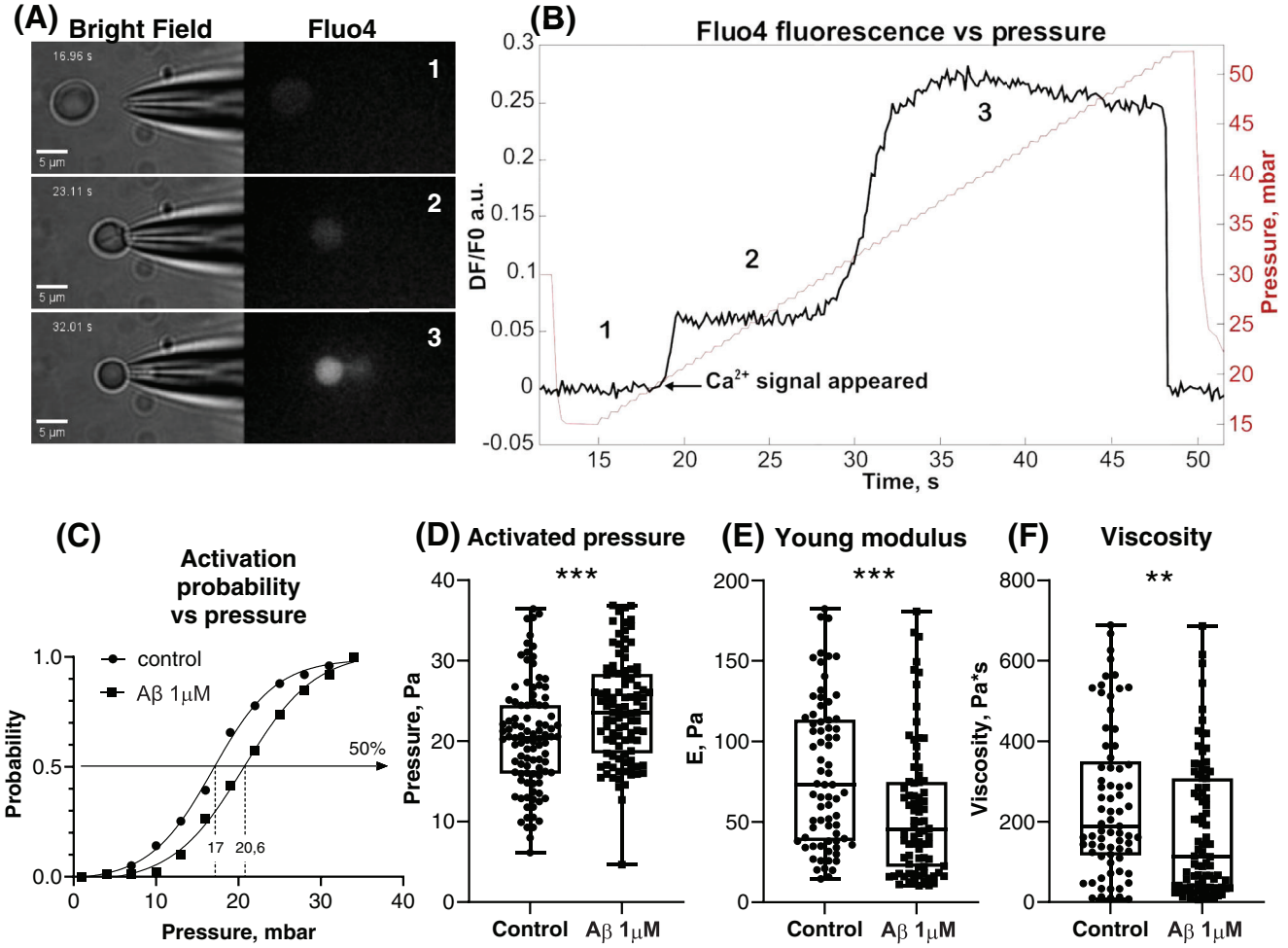

FIGURE 1 Aβ changes biomechanical properties of RBC membrane. (A) Visual representation of the experimental technique. (B) Graphical representation of experimental technique. Pressure gradually increased by 0.5 mbar. (C) Fitting curve representing the activation probability for a given pressure in case of control (circles) and Aβ (squares) preincubated samples. (D) Boxplots representing activated pressure values for control and preincubated with 1 µM Aβ populations of RBCs. N(control) = 99, N(Aβ) = 99. (E) Boxplots representing Young's modulus values for control and preincubated with 1 µM Aβ populations of RBCs. N(control) = 73, N(Aβ) = 87. (F) Boxplots representing viscosity values for control and preincubated with 1 µM Aβ populations of RBCs. N(control) = 73, N(Aβ) = 87. For the box-and-whisker plots, the horizontal bar shows the median, and the upper and lower boundaries show the min and max values, respectively. Mann-Whitney U-test, $^{**}p < 0.01$, $^{***}p < 0.001$. Aβ, beta-amyloid protein; RBC, red blood cell.

membrane irregularities such as appearance of spikes during shrinkage of the cell, while FSC represents cell size changes under Yoda1 application (Figure 4A). Quantification of the relative difference between the baseline (BL) and Yoda1 exposure revealed a significant increase in the SSC and decrease in the FSC upon Yoda1 exposure (Figure S2). Moreover, AD patients showed significant increase in percentage of both SSC and FSC compared to HCs. The elevation in SSC was significantly increased also in patients with MCI compared to HCs (Figure 4).

3.5 | AD patients show an expected increase in the conventional AD-biomarkers

To evaluate whether the Yoda1-induced Ca^{2+} flux in RBCs outperforms the conventional AD biomarkers 42 and 40 amino acid-long amyloid β (Aβ42 and Aβ40), tau phosphorylated at amino acid 231 (pTau-231),[33,41] GFAP, and NfL in plasma,[12,13,16] we measured the concentrations of Aβ42, Aβ40, pTau-231, GFAP, and NfL concentrations in plasma samples of patients using highly sensitive Single molecule array (Simoa) assays (Figure 5, Table 1). Our data confirm the expected, significantly lower levels of Aβ42 and the ratio of Aβ42 and Aβ40 in AD patients compared to HCs. Also, the concentrations of GFAP and NfL, markers of astrocytic activation and neurodegeneration, respectively, were significantly higher in AD patients compared to HCs. None of the biomarkers showed alterations in patients with MCI. Together, this profile of biomarkers confirmed the clinical diagnosis of AD.

3.6 | Interaction analysis

We used a machine learning algorithm to evaluate whether the Ca^{2+} flux in RBCs outperforms the measurement of conventional

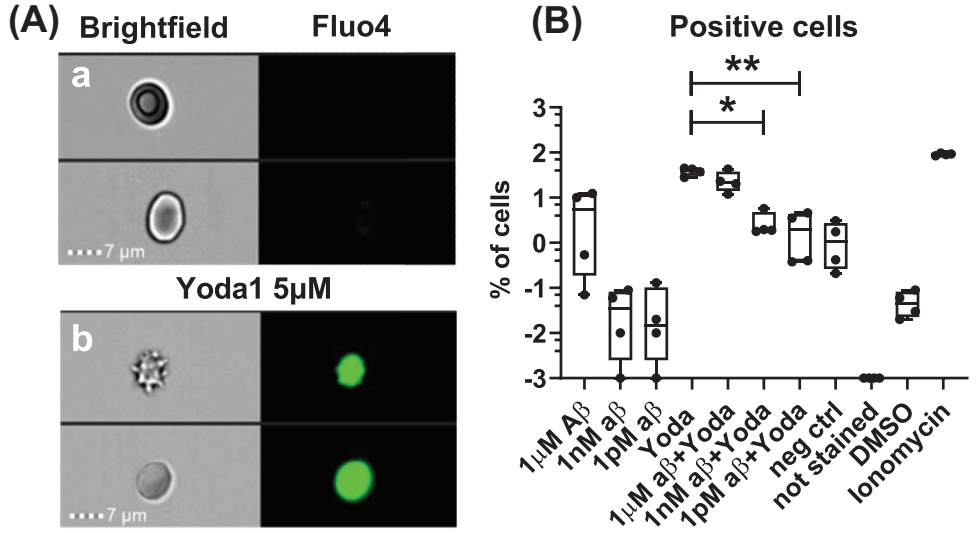

FIGURE 2 Aβ preincubation decreasing Yoda1-activated positive cells. (A) Visual presentation of non-activated (a) and Yoda1 5 µM activated (b) RBCs in flow cytometry stream. (B) Box-and-whiskers plots of cell responded to Yoda1 5 µM application in RBCs that were incubated (or not) 20 min with Aβ protein in different concentrations for 20 min prior to flow recording. Ionomycin was used as a positive control. For the box-and-whisker plots, the horizontal bar shows the median, and the upper and lower boundaries show the min and max values, respectively. *N* (samples) = 4, Kruskal-Wallis test, $^{*}p < 0.05$, $^{**}p < 0.01$. Aβ, beta-amyloid protein; RBC, red blood cell.

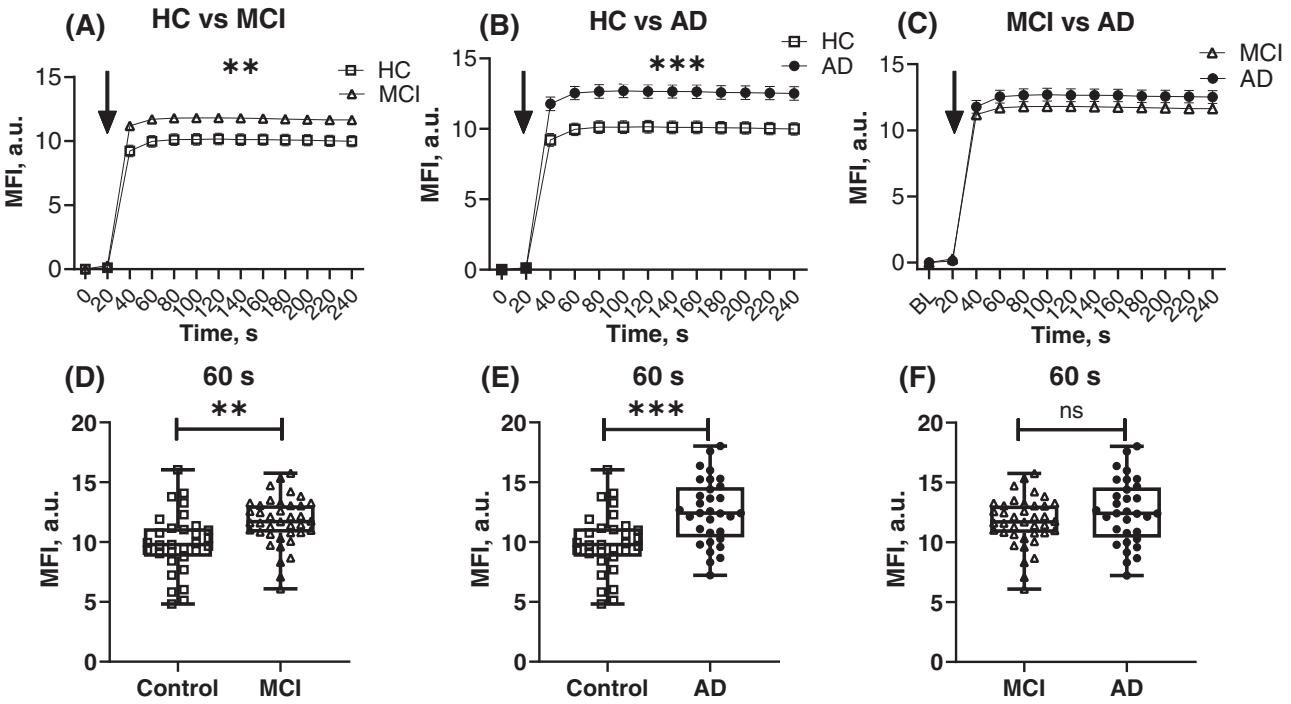

FIGURE 3 Yoda1-induced activation of Piezo1 receptors in human RBC. Activation of Piezo1 receptors presented as normalized on baseline values of Fluo4 median fluorescence intensity (MFI) induced by 5 µM Yoda1 agonist in RBCs of groups of patients: HC versus MCI patients (**A**), HC versus AD patients (**B**), and MCI versus AD patients (C) the time-course of changes in MFI. The moment of Yoda1 application marked with an arrow. (D-F) Box-and-whiskers plots showing Fluo-4 fluorescence at 60 s in the presence of Yoda1 5 µM. For the box-and-whisker plots, the horizontal bar shows the median, and the upper and lower boundaries show the min and max values, respectively. $^{*}p < 0.05$, $^{***}p < 0.001$ [*n* (control) = 31, n(MCI) = 39, *n*(AD) = 32, two-way ANOVA, followed by Bonferroni's multiple comparison test]. ANOVA, analysis of variance; MCI, mild cognitive impairment; RBC, red blood cell.

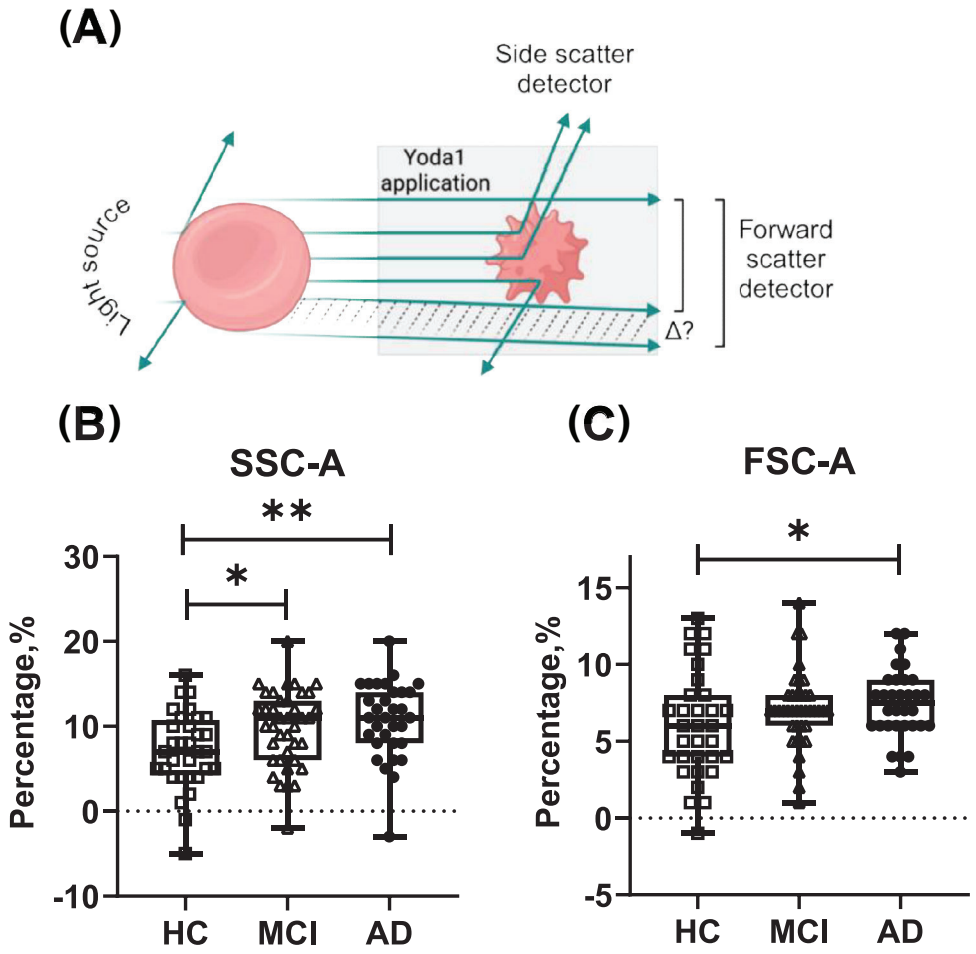

FIGURE 4 Changes in optical measurements after Piezo1 receptors activation in human RBC. (A) Schematic presentation of alterations in scattered parameters of RBCs after Yoda1 application. Created with Biorender.com (B) SSC-A and (C) FSC-A differences in HC, MCI, and AD patients' RBCs. Every box-and-whiskers plot dot is showing percentage differences between BL signal and Yoda1 treated signal within one RBC sample Ca^{2+} recording. For the box-and-whisker plots, the horizontal bar shows the median, and the upper and lower boundaries show the min and max values, respectively. $^{*}p < 0.05$, $^{**}p < 0.01$ [n (control) = 31, n(MCI) = 39, n(AD) = 32, ANOVA, followed by Bonferroni's multiple comparison test].

AD biomarkers in plasma and provides additional benefit for clinicians in diagnosing patients with early AD-related dementia. Since the diagnosis procedure also includes a variety of clinical information in addition to the conventional AD biomarkers, we used this entire dataset of patient information covering a broad range of the parameters related to patient apolipoprotein E (*APOE*) status, demographic characteristics, clinical measurements (Table S1), confirmed comorbidities, MRI parameters, CERAD parameters, and lifestyle parameters (Table 2). The random forest classifier was ran twice using five-fold cross-validation to train the model on known patients and to test whether it could distinguish unknown patients. Together with the measured biomarker concentrations (Aβ40, Aβ42, NfL, GFAP, pTau231) and known classification of patients provided by hospital, an in-depth analysis of Yoda1-induced Ca^{2+} signals (maximum values of the median 5 μM Yoda1 signal) was conducted.

The random forest classifier demonstrated strong performance, getting areas under curves (AUCs) of 0.81, 0.78, and 0.60 for AD, HC, and MCI, respectively (Figure 6A). This indicates robust predictive capability for AD and HC, but less for MCI.

Feature importance analysis revealed Yoda1-induced Ca^{2+} flux as the most predictive feature, particularly for distinguishing MCI from HC (Figure 6B). While CERAD memory test variables and left hippocampal volume were also found important for the classification of AD patients and HCs, they were less predictive for MCI. Notably, Yoda1-induced Ca^{2+} flux was the only feature significantly contributing to recognition of MCI.

Combining Yoda1-induced Ca^{2+} flux with features such as memory scores and MRI measurements further improved the model classification (Figure 6C). The proximity matrix also showed distinct clustering of AD, MCI, and HC, albeit with some overlap attributed to the dimensionality reduction (i.e., from 47 dimensions of the feature space to 2) (Figure 6D). Removing Yoda1-induced Ca^{2+} flux resulted in a 10% decrease in the performance, underscoring the importance of this parameter in the classification of the patients. Precisely, AUCs dropped to 0.78, 0.72, and 0.53 for AD, HC, and MCI, respectively, highlighting the challenge of detecting MCI without an effective

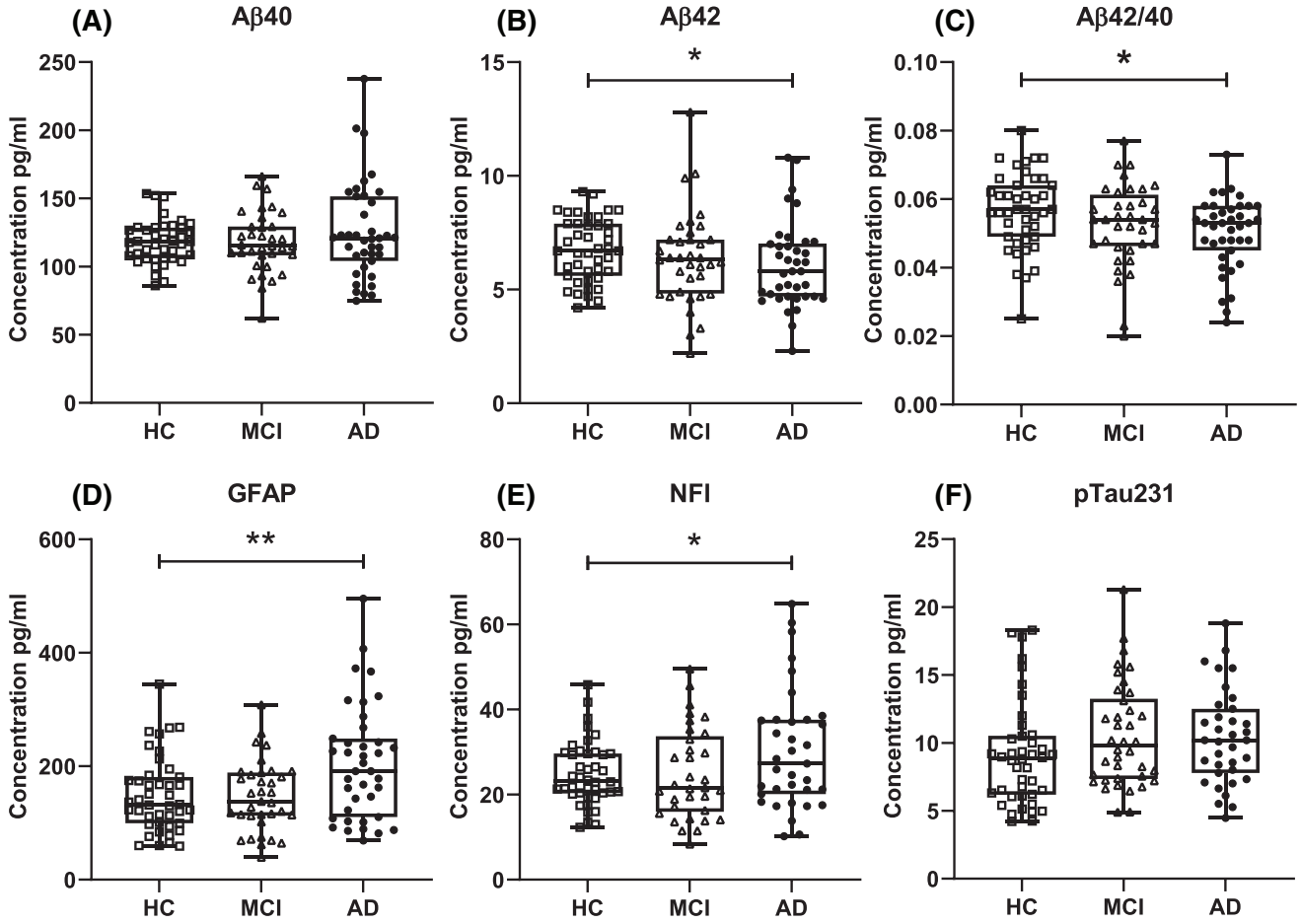

FIGURE 5 Plasma biomarkers characteristics of APOLLO cohort. (A) Aβ40, (B) Aβ42, (D) GFAP, (E) NfL, (F) pTau231 plasma concentrations of individuals across the AD, MCI, and HC cases. The box-and-whisker plots show plasma concentrations of chosen biomarkers across groups. For the box-and-whisker plots, the horizontal bar shows the median, and the upper and lower boundaries show the min and max values, respectively. Statistical outliers have been removed using GraphPad Prism 10. *p* values indicate the results of the Kruskal-Wallis test with Dunn's multiple comparisons test at $^{*}p < 0.05$, $^{**}p < 0.01$. Aβ40, beta-amyloid peptide; GFAP, glial fibrillary acidic protein; HC, healthy controls; MCI, mild cognitive impairment; NfL, neurofilament light chain.

biomarker. Thus, Piezo1 has a superior value in predicting AD-related dementia (Figure S4).

3.7 | Limitation

The limitation of the current study is the lack of CSF and PET measurements of patients, making it impossible to link the Piezo1 measurements with CSF data and PET.[42] In addition, due to the rather small group of patients, our ability to detect associations between the clinical parameters and Ca^{2+} responses is limited, and our interpretation of the correlation analysis should be viewed with caution.

4 | DISCUSSION

Here, we report enhanced Yoda1-induced Ca^{2+} flux, indicative of increased Piezo1 sensitivity, in human RBCs as a feature associated with early AD-related dementia. We also provide a mechanistic explanation for the enhanced Yoda1-induced Ca^{2+} flux in patients with AD.

We modeled Aβ-induced alterations in the biomechanical properties of RBCs. During aspiration, RBC experienced mechanical stress followed by increase in the Ca^{2+} flux through Piezo1 channels. While the initial Ca^{2+} influx can be attributed to Piezo1 channel activation, the secondary elevation in the fluorescent signal observed in our measurements suggest that additional mechanisms may be involved. One possible explanation is that Piezo1 activation triggers Gárdos channel-mediated membrane potential flickering, which in turn activates the voltage-dependent Ca^{2+} channel Cav2.1. Such mechanism has been previously described in RBCs[43] and could contribute to the sustained Ca^{2+} rise observed in our study. Further investigations are needed to confirm this hypothesis and elucidate its potential implications for RBC deformability and microcirculatory efficiency.

Our findings showed decreased Young's modulus indicating a partial loss of membrane stiffness. This decreased stiffness results in an

TABLE 2 Characteristics of the APOLLO cohort.

Characteristic	All patients (102)	HC (31)	MCI (39)	AD (32)
Age (mean ± SD)	70.60 ± 6.81	70.65 ± 5.68	70.38 ± 6.70	70.81 ± 8.03
Gender (females, %)	45.10	74.19	28.21	37.50
APOE carriers (2.3/3.3/3.4/4.4/not reported, %)	0.98/40.20/26.47/14.71/17.65	0/51.61/32.26/3.23/12.90	2.56/46.15/28.21/5.13/17.95	0/25/28.13/37.50/9.38
Hypertension (yes/no/not reported, %)	46.1/51/2.9	41.94/54.84/3.23	58.97/41.03/0	34.38/59.38/6.25
Hypercholesterolemia (yes/no/not reported, %)	53.92/43.14/2.94	45.16/51.61/3.23	56.41/43.59/0	59.38/34.38/6.25
Diabetes (yes/no/not reported, %)	11.76/85.29/2.94	6.45/90.32/3.23	17.95/82.05/0	9.38/84.38/6.25
Cancer (yes/no/not reported, %)	2.94/94.12/2.94	3.23/93.55/3.23	0/0/0	6.25/87.50/6.25
Migraine (yes/no/not reported, %)	11.76/85.29/2.94	19.35/77.42/3.23	5.13/94.87/0	12.50/81.25/6.25
Heart/vascular disorders (yes/no/not reported, %)	34.31/62.75/2.94	45.16/51.61/3.23	28.21/71.79/0	31.25/62.50/6.25
Smoking (never/quitted/sometimes/constantly	58.82/37.25/2.94/0.98	51.61/45.16/3.23/0	64.10/33.33/2.56/0	59.38/34.38/6.25/0
Drinking (never/occasionally/recently increased/problem use)	28.43/64.71/4.9/1.96	25.81/67.41/6.45/0	28.21/66.67/2.56/2.56	31.25/59.38/6.25/3.13

Abbreviations: AD, Alzheimer's disease; APOE, apolipoprotein E; HC, healthy control; MCI, mild cognitive impairment.

increased deformability during aspiration by micropipette: the cell acquires a more liquid-like behavior, reducing viscosity and requires higher activation pressure to achieve the same Yoda1-induced fluorescent signal as for untreated RBCs. At the same time, incubation of RBCs with Aβ blocked the proper Yoda1-induced activation of Piezo1 channel. This simple and rough model demonstrates increased deformability that is crucial for the microcirculatory capacity of RBCs. Indeed, prior studies have shown alterations in the biochemical properties of RBCs of AD patients.[44]

Recent advances in analytical methodologies, notably mass spectrometry, and single-molecule immunoassays, which boast enhanced sensitivity for detecting Aβ at min concentrations, have disclosed a decrease in plasma Aβ42/Aβ40 ratios of less than 20% in individuals manifesting cerebral Aβ pathology as compared to healthy individuals.[13] Aβ protein can fold easily and aggregate a fibrillar form on the surface of the RBCs of AD-confirmed patients.[26] AD patients have been reported to have lower plasma Aβ levels compared to HC. We hypothesize that this is reflected as less Aβ-induced blockage in Piezo1 resulting in higher Yoda1-induced Ca^{2+} flux in individuals with AD and higher deformability of AD patients' RBCs, which has been demonstrated in our flow cytometry experiments. Indeed, it is well established that Piezo1 channel-mediated Ca^{2+} flux contributes greatly in RBC volume homeostasis and physiology,[2] and it has been demonstrated that small concentrations of Aβ are able to block the proper function of Piezo1 channel in multiple different cell types.[6,9,45] Here, we provide evidence that this phenomenon may extend to RBCs. However, Aβ is also known to interact with and alter membrane lipid composition.[46–48] Lipid-fibril interaction,[46] Aβ oligomer toxicity,[49] and Aβ-induced production of reactive oxygen spieces[50] may all impact RBC membrane properties and thus Piezo1 channel activity. These changes in the lipid environment could be another possible explanation for the increased Piezo1 activity observed in AD patients. Further research is needed to explore this aspect in detail, and is beyond the scope of this study.

Interaction analysis performed based on the medical information of the patients demonstrated that Yoda1-induced Ca^{2+} flux provides significant benefit in detecting MCI and AD cases from HC. This parameter was crucial for identifying AD and was the only variable that significantly aided the identification of patients with MCI. In addition, Yoda1-induced Ca^{2+} response parameter showed significant AD predictive capacity in the performance analysis. Interestingly, exclusion of this parameter from the classifier decreased its performance with 10%, underscoring the importance of Yoda1-induced Ca^{2+} response in predicting AD-related dementia.

None of the comorbidities or blood parameters had a significant contribution to the patient classification in our analyzed cohort. This may be due to the fact that patients included in this study had well-managed comorbid conditions, which can be confirmed by their clinical blood test data. It is conceivable that these individuals are undergoing treatment regimens that effectively maintain the pertinent hematological parameters associated with their comorbidities within the normal range. Consequently, it is reasonable to infer that these comorbidities do not exert a substantive impact on the principal mechanistic pathway under investigation in this study. However, in general, it has been shown that diabetes and vascular disorders may alter the proper function of Piezo1 channel.[51]

Summarizing our findings, we suggest that Yoda1-induced Ca^{2+} flux emerges as a measurable indicator associated with and improves the detection of AD-related dementia.

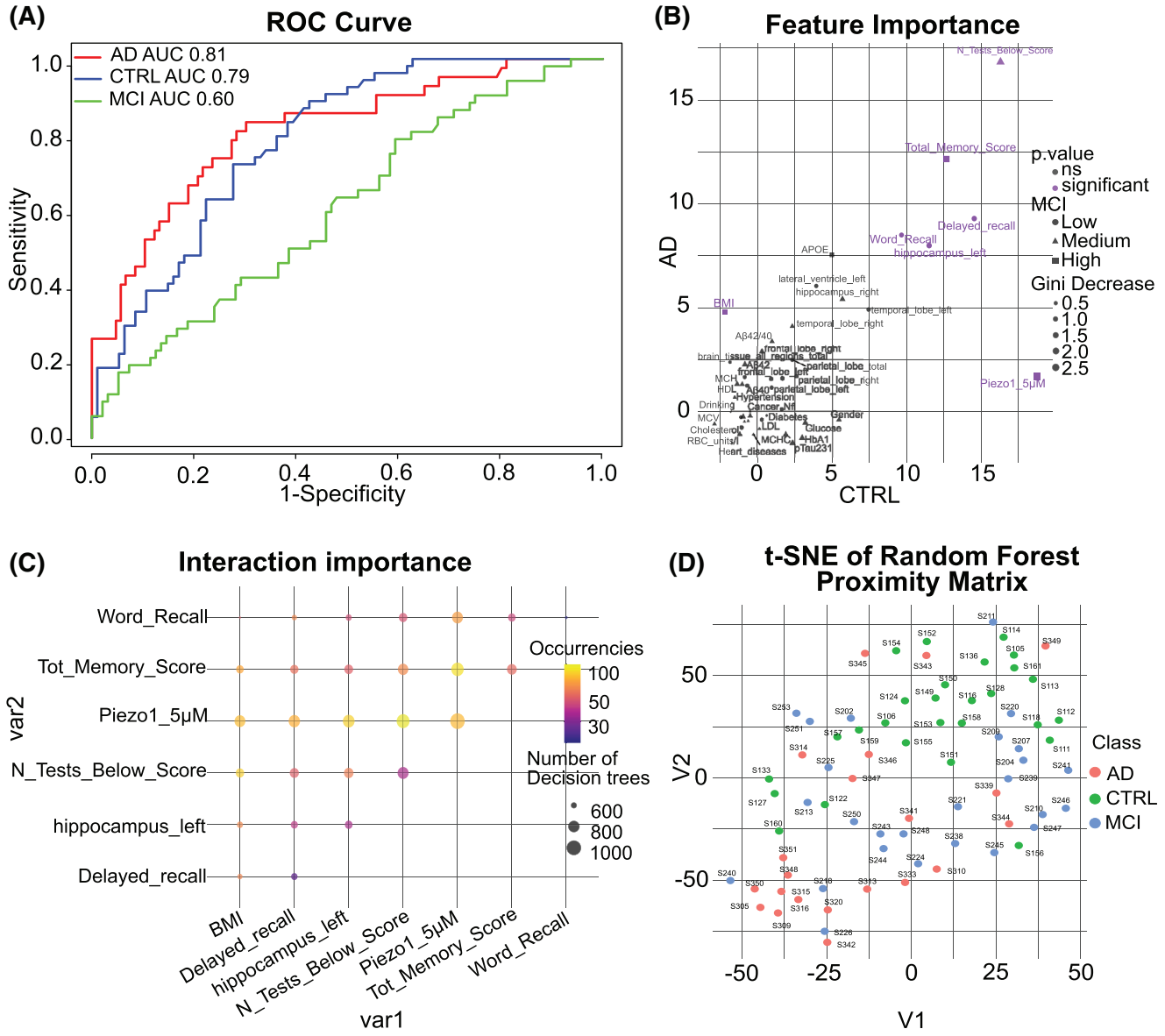

FIGURE 6 Results of the patient classification using a random forest model. (A) The receiver operating characteristic (ROC) curves, illustrating the model's performance in distinguishing Alzheimer's disease (AD), controls, and mild cognitive impairment (MCI) based on the area under the curve (AUC). (B) The importance of individual features in the classification of each patient class, measured by Gini decrease and p-value. Precisely, the point size is related to the overall Gini decrease of the feature, while axis and shape are related to the Gini decrease of the feature for each specific class (i.e., more the point is at the right and more important for recognizing control patients). (C) The importance of feature interactions, represented by the frequency of co-occurrence within the random forest's decision trees. (D) The t-distributed Stochastic Neighbor Embedding (t-SNE) representation of the random forest proximity matrix, revealing the similarity between individual patient samples based on their feature values and assigned class.

AUTHOR CONTRIBUTIONS

Conceptualization: Tarja M. Malm, Rashid Giniatullin, Valeriia Sitnikova. *Methodology*: Valeriia Sitnikova, Dilyara Nurkhametova, Nicoletta Braidotti, Luca Giudice. *Investigation*: Valeriia Sitnikova, Dilyara Nurkhametova, Nicoletta Braidotti, Catalin D. Ciubotaru, Luca Giudice, Ulla Impola, Sari Kärkkäinen, Juho Kalapudas, Ilkka Fagerlund, Henrik Zetterberg. *Visualization*: Valeriia Sitnikova, Dilyara Nurkhametova, Nicoletta Braidotti, Catalin D. Ciubotaru, Luca Giudice, Ulla Impola. *Data validation*: Dan Cojoc, Anne Koivisto, Saara Laitinen, Tarja Kokkola, Henrik Zetterberg. *Contribution to patient samples and data*: Anne Koivisto, Katja M. Kanninen, Tarja M. Malm, Elina Penttilä, Heikki Löppönen. *Supervision and planning*: Tarja M. Malm, Rashid Giniatullin. *Writing original draft*: Valeriia Sitnikova, Tarja M. Malm. *Reviewing and editing*: All authors.

ACKNOWLEDGMENTS

The authors thank prof. Igor Kudryavtsev from Institute of Experimental Medicine (RAS) Saint Petersburg, Russia, for help in set up of flow cytometry protocol and staff scientist Petri Mäkinen from University of Eastern Finland for practical advices according the flow

cytometry and device service work. They want to acknowledge technicians from Malm group, Ylli Torn, and Hanna Härkönen, for help with sample transportation, processing and storage and from Biomarker Laboratory, Päivi Räsänen, for help with Simoa analysis performance. They acknowledge all the people donated their blood from the Red Cross of Finland (Helsinki) and Italy (Trieste) and all the patients (APOLLO) agreed to participate our research.

Open access publishing facilitated by Ita-Suomen yliopisto, as part of the Wiley - FinELib agreement.

This work is supported by Business Finland and Academy of Finland (to T.M.). H.Z. is a Wallenberg Scholar, and a Distinguished Professor at the Swedish Research Council supported by grants from the Swedish Research Council (#2023-00356, #2022-01018 and #2019-02397), the European Union's Horizon Europe research and innovation programme under grant agreement No. 101053962, and Swedish State Support for Clinical Research (#ALFGBG-71320).

The AD patient's blood sampling and usage has been approved by the Regional Medical Research Ethics Committee of the Wellbeing Services County of North Savo (536/13.02.00/2017). The patients/participants provided their written informed consent to participate in this study.

CONFLICT OF INTEREST STATEMENT

Henrik Zetterberg has served at scientific advisory boards and/or as a consultant for Abbvie, Acumen, Alector, Alzinova, ALZpath, Amylyx, Annexon, Apellis, Artery Therapeutics, AZTherapies, Cognito Therapeutics, CogRx, Denali, Eisai, LabCorp, Merry Life, Nervgen, Novo Nordisk, Optoceutics, Passage Bio, Pinteon Therapeutics, Prothena, Red Abbey Labs, reMYND, Roche, Samumed, Siemens Healthineers, Triplet Therapeutics, and Wave, has given lectures sponsored by Alzecure, BioArctic, Biogen, Cellectricon, Fujirebio, Lilly, Novo Nordisk, Roche, and WebMD, and is a co-founder of Brain Biomarker Solutions in Gothenburg AB (BBS), which is a part of the GU Ventures Incubator Program (outside submitted work).

Tarja M. Malm, Rashid Giniatullin, Dilyara Nurkhametova, and Ilkka Fagerlund are inventors of a patent related to this study.

Valeriia Sitnikova and the rest of the co-authors have nothing to disclose.

DATA AVAILABILITY STATEMENT

The data generated in this study are available upon request from the corresponding authors. All data needed to evaluate the conclusions in the article are present in the article and/or the Supplementary Materials.

ETHICS STATEMENT

Regional Medical Research Ethics Committee of the Wellbeing Services County of North Savo approval 536/13.02.00/2017.

ORCID

Valeriia Sitnikova https://orcid.org/0000-0002-8192-1236

REFERENCES

1. Moras M, Lefevre SD, Ostuni MA. From erythroblasts to mature red blood cells: organelle clearance in mammals. *Front Physiol* 2017;8:318979. doi:10.3389/FPHYS.2017.01076/BIBTEX
2. Cahalan SM, Lukacs V, Ranade SS, Chien S, Bandell M, Patapoutian A. Piezo1 links mechanical forces to red blood cell volume. *Elife*. 2015;4. doi:10.7554/eLife.07370
3. Svetina S, Švelc Kebe T, Božič B. A model of Piezo1-based regulation of red blood cell volume. *Biophys J*. 2019;116:151-164. doi:10.1016/j.bpj.2018.11.3130
4. Lew VL, Tiffert T. On the mechanism of human red blood cell longevity: roles of calcium, the sodium pump, PIEZO1, and gardos channels. *Front Physiol*. 2017;8:311944. doi:10.3389/FPHYS.2017.00977/BIBTEX
5. Vaisey G, Banerjee P, North AJ, Haselwandter CA, Mackinnon R. Piezo1 as a force-through-membrane sensor in red blood cells. *Elife*. 2022;11:e82621. doi:10.7554/ELIFE.82621
6. Jäntti H, Sitnikova V, Ishchenko Y, et al. Microglial amyloid beta clearance is driven by PIEZO1 channels. *J Neuroinflammation*. 2022;19. doi:10.1186/s12974-022-02486-y
7. Hu J, Chen Q, Zhu H, et al. Microglial Piezo1 senses Aβ fibril stiffness to restrict Alzheimer's disease. *Neuron*. 2023;111:15-29. doi:10.1016/J.NEURON.2022.10.021. e8.
8. Velasco-Estevez M, Rolle SO, Mampay M, Dev KK, Sheridan GK. Piezo1 regulates calcium oscillations and cytokine release from astrocytes. *Glia*. 2020;68:145-160. doi:10.1002/glia.23709
9. Maneshi MM, Ziegler L, Sachs F, Hua SZ, Gottlieb PA. Enantiomeric Aβ peptides inhibit the fluid shear stress response of PIEZO1. *Sci Rep*. 2018;8. doi:10.1038/s41598-018-32572-2
10. Velasco-Estevez M, Mampay M, Boutin H, et al. Infection augments expression of mechanosensing Piezo1 channels in amyloid plaque-reactive astrocytes. *Front Aging Neurosci*. 2018;10:332. doi:10.3389/fnagi.2018.00332
11. Mo JA, Lim JH, Sul AR, Lee M, Youn YC, Kim HJ. Cerebrospinal fluid β-Amyloid1-42 Levels in the differential diagnosis of Alzheimer's disease—systematic review and meta-analysis. *PLoS One*. 2015;10:e0116802. doi:10.1371/JOURNAL.PONE.0116802
12. Olsson B, Lautner R, Andreasson U, et al. CSF and blood biomarkers for the diagnosis of Alzheimer's disease: a systematic review and meta-analysis. *Lancet Neurol*. 2016;15:673-684. doi:10.1016/S1474-4422(16)00070-3
13. Teunissen CE, Verberk IMW, Thijssen EH, et al. Blood-based biomarkers for Alzheimer's disease: towards clinical implementation. *Lancet Neurol*. 2022;21:66-77. doi:10.1016/S1474-4422(21)00361-6
14. Kuo YM, Kokjohn TA, Kalback W, et al. Amyloid-β peptides interact with plasma proteins and erythrocytes: implications for their quantitation in plasma. *Biochem Biophys Res Commun*. 2000;268:750-756. doi:10.1006/bbrc.2000.2222
15. Lövheim H, Elgh F, Johansson A, et al. Plasma concentrations of free amyloid β cannot predict the development of Alzheimer's disease. *Alzheimers Dement*. 2017;13:778-782. doi:10.1016/j.jalz.2016.12.004
16. Schindler SE, Karikari TK, Ashton NJ, et al. Effect of race on prediction of brain amyloidosis by plasma Aβ42/Aβ40, phosphorylated tau, and neurofilament light. *Neurology*. 2022;99. 10.1212/WNL.0000000000200358
17. Svetina S. Theoretical bases for the role of red blood cell shape in the regulation of its volume. *Front Physiol*. 2020;11:527131. doi:10.3389/fphys.2020.00544
18. Evtugina NG, Peshkova AD, Khabirova AI, et al. Activation of Piezo1 channels in compressed red blood cells augments platelet-driven contraction of blood clots. *J Thromb Haemost*. 2023;21:2418-2429. doi:10.1016/j.jtha.2023.05.022
19. Lohia R, Allegrini B, Berry L, et al. Pharmacological activation of PIEZO1 in human red blood cells prevents Plasmodium falciparum

invasion. *Cell Mol Life Sci*. 2023;80:124. doi:10.1007/s00018-023-04773-0
20. Nelson AR, Sweeney MD, Sagare AP. Zlokovic B V. Neurovascular dysfunction and neurodegeneration in dementia and Alzheimer's disease. *Biochim Biophys Acta Mol Basis Dis*. 2016;1862:887-900. doi:10.1016/j.bbadis.2015.12.016
21. Shin Y, Choi SH, Kim E, et al. Blood–brain barrier dysfunction in a 3D in vitro model of Alzheimer's disease. *Adv Sci*. 2019;6:1900962. doi:10.1002/advs.201900962
22. Yamaguchi Y, Allegrini B, Rapetti-Mauss R, et al. Hereditary xerocytosis: differential behavior of PIEZO1 mutations in the N-terminal extracellular domain between red blood cells and HEK cells. *Front Physiol*. 2021;12:736585. doi:10.3389/fphys.2021.736585
23. Kiko T, Nakagawa K, Satoh A, et al. Amyloid β levels in human red blood cells. *PLoS One*. 2012;7. doi:10.1371/JOURNAL.PONE.0049620
24. Carelli-Alinovi C, Dinarelli S, Sampaolese B, Misiti F, Girasole M. Morphological changes induced in erythrocyte by amyloid beta peptide and glucose depletion: a combined atomic force microscopy and biochemical study. *Biochim Biophys Acta Biomembr*. 2019;1861:236-244. doi:10.1016/j.bbamem.2018.07.009
25. Kosenko EA, Tikhonova LA, Montoliu C, Barreto GE, Aliev G, Kaminsky YG. Metabolic abnormalities of erythrocytes as a risk factor for Alzheimer's disease. *Front Neurosci*. 2018;11:324015. doi:10.3389/FNINS.2017.00728/BIBTEX
26. Nirmalraj PN, Schneider T, Felbecker A. Spatial organization of protein aggregates on red blood cells as physical biomarkers of Alzheimer's disease pathology. *Sci Adv*. 2021;7. doi:10.1126/sciadv.abj2137
27. Lan J, Liu J, Zhao Z, et al. The peripheral blood of Aβ binding RBC as a biomarker for diagnosis of Alzheimer's disease. *Age Ageing*. 2015;44:458-464. doi:10.1093/ageing/afv009
28. Piccarducci R, Caselli MC, Zappelli E, et al. The role of amyloid-β, tau, and α-Synuclein proteins as putative blood biomarkers in patients with cerebral amyloid angiopathy. *J Alzheimers Dis*. 2022;89:1039-1049. doi:10.3233/JAD-220216
29. Jack CR, Albert MS, Knopman DS, et al. Introduction to revised criteria for the diagnosis of Alzheimer's disease: National Institute on Aging and the Alzheimer Association Workgroups. *Alzheimers Dement*. 2011;7:257. doi:10.1016/J.JALZ.2011.03.004
30. Fillenbaum GG, Mohs R. CERAD (Consortium to Establish a Registry for Alzheimer's Disease) Neuropsychology Assessment Battery: 35 years and counting. *J Alzheimers Dis*. 2023;93:1-27. doi:10.3233/JAD-230026
31. Alenius M, Ngandu T, Koskinen S, et al. Education-based cutoffs for cognitive screening of Alzheimer's disease. *Dement Geriatr Cogn Disord*. 2022;51:42-55. doi:10.1159/000521982
32. Tzur A, Moore JK, Jorgensen P, Shapiro HM, Kirschner MW. Optimizing optical flow cytometry for cell volume-based sorting and analysis. *PLoS One*. 2011;6:16053. doi:10.1371/journal.pone.0016053
33. Ashton NJ, Pascoal TA, Karikari TK, et al. Plasma p-tau231: a new biomarker for incipient Alzheimer's disease pathology. *Acta Neuropathol*. 2021;141:709-724. doi:10.1007/s00401-021-02275-6
34. Braidotti N, Ciubotaru CD, Rizzo D, Bergamo L, Bernareggi A, Cojoc D. Investigating mechanosensitive channels activation in concert with the mechanical properties of red blood cells. *Discover Mech Eng*. 2023;2:18. doi:10.1007/s44245-023-00026-3
35. Kuhn M. Building predictive models in R using the caret package. *J Stat Softw*. 2008;28:1-26. doi:10.18637/JSS.V028.I05
36. Breiman L. Random forests. *Mach Learn*. 2001;45:5-32. doi:10.1023/A:1010933404324/METRICS
37. Stekhoven DJ, Bühlmann P, Data and text mining MissForest-nonparametric missing value imputation for mixed-type data. *Bioinformatics*. 2012;28:112-118. doi:10.1093/bioinformatics/btr597
38. Azur MJ, Stuart EA, Frangakis C, Leaf PJ. Multiple imputation by chained equations: what is it and how does it work?. *Int J Methods Psychiatr Res*. 2011;20:40. doi:10.1002/MPR.329
39. Evans E, Yeung A. Apparent viscosity and cortical tension of blood granulocytes determined by micropipet aspiration. *Biophys J*. 1989;56:151-160. doi:10.1016/S0006-3495(89)82660-8
40. Hochmuth RM. Micropipette aspiration of living cells. *J Biomech*. 2000;33:15-22. doi:10.1016/S0021-9290(99)00175-X
41. Milà-Alomà M, Ashton NJ, Shekari M, et al. Plasma p-tau231 and p-tau217 as state markers of amyloid-β pathology in preclinical Alzheimer's disease. *Nat Med*. 2022;28:1797-1801. doi:10.1038/s41591-022-01925-w
42. Jack CR, Andrews JS, Beach TG, et al. Revised criteria for diagnosis and staging of Alzheimer's disease: Alzheimer's Association Workgroup. *Alzheimers Dement*. 2024;20:5143-5169. doi:10.1002/ALZ.13859
43. Jansen J, Qiao M, Hertz L, et al. Mechanistic ion channel interactions in red cells of patients with Gárdos channelopathy. *Blood Adv*. 2021;5:3303. doi:10.1182/BLOODADVANCES.2020003823
44. Nardini M, Ciasca G, Lauria A, et al. Sensing red blood cell nanomechanics: toward a novel blood biomarker for Alzheimer's disease. *Front Aging Neurosci*. 2022;14:932354. doi:10.3389/FNAGI.2022.932354/BIBTEX
45. Hu J, Chen Q, Zhu H, Wang B, Zhang L. Mo Correspondence W. Microglial Piezo1 senses Aβ fibril stiffness to restrict Alzheimer's disease. *Neuron*. 2023;111:15-29. doi:10.1016/j.neuron.2022.10.021.e8.
46. Lindberg DJ, Wesén E, Björkeroth J, Rocha S, Esbjörner EK. Lipid membranes catalyse the fibril formation of the amyloid-β (1-42) peptide through lipid-fibril interactions that reinforce secondary pathways. *Biochim Biophys Acta (BBA)—Biomembranes*. 2017;1859:1921-1929. doi:10.1016/J.BBAMEM.2017.05.012
47. Hashimoto M, Hossain S, Katakura M, Al Mamun A, Shido O. The binding of Aβ1-42 to lipid rafts of RBC is enhanced by dietary docosahexaenoic acid in rats: implicates to Alzheimer's disease. *Biochim Biophys Acta (BBA)—Biomembranes*. 2015;1848:1402-1409. doi:10.1016/J.BBAMEM.2015.03.008
48. Hu N, Gao L, Jiang Y, et al. The relationship between blood lipids and plasma amyloid beta is depend on blood pressure: a population-based cross-sectional study. *Lipids Health Dis*. 2020;19:8. doi:10.1186/S12944-020-1191-4
49. Sengupta U, Nilson AN, Kayed R. The role of amyloid-β oligomers in toxicity, propagation, and immunotherapy. *EBioMedicine*. 2016;6:42-49. doi:10.1016/j.ebiom.2016.03.035
50. Nakagawa K, Kiko T, Miyazawa T, et al. Amyloid β-induced erythrocytic damage and its attenuation by carotenoids. *FEBS Lett*. 2011;585:1249-1254. doi:10.1016/J.FEBSLET.2011.03.060
51. Zhu W, Guo S, Homilius M, et al. PIEZO1 mediates a mechanothrombotic pathway in diabetes. *Sci Transl Med*. 2022;14. doi:10.1126/scitranslmed.abk1707

SUPPORTING INFORMATION

Additional supporting information can be found online in the Supporting Information section at the end of this article.

How to cite this article: Sitnikova V, Nurkhametova D, Braidotti N, et al. Increased activity of Piezo1 channel in red blood cells is associated with Alzheimer's disease-related dementia. *Alzheimer's Dement*. 2025;21:e70368. https://doi.org/10.1002/alz.70368